

Properties of collective flow and pion production in intermediate-energy heavy-ion collisions with a relativistic quantum molecular dynamics model*

Si-Na Wei¹ and Zhao-Qing Feng^{1,†}

¹*School of Physics and Optoelectronics, South China University of Technology, Guangzhou 510640, China*

The relativistic mean-field approach was implemented in the Lanzhou quantum molecular dynamics transport model (LQMD.RMF). Using the LQMD.RMF, the properties of collective flow and pion production were investigated systematically for nuclear reactions with various isospin asymmetries. The directed and elliptic flows of the LQMD.RMF are able to describe the experimental data of STAR Collaboration. The directed flow difference between free neutrons and protons was associated with the stiffness of the symmetry energy, that is, a softer symmetry energy led to a larger flow difference. For various collision energies, the ratio between the π^- and π^+ yields increased with a decrease in the slope parameter of the symmetry energy. When the collision energy was 270 MeV/nucleon, the single ratio of the pion transverse momentum spectra also increased with decreasing slope parameter of the symmetry energy in both nearly symmetric and neutron-rich systems. However, it remained difficult to determine the dependence of the double ratio on the stiffness of the symmetry energy.

Keywords: Heavy-ion collision, Collective flow, Pion production, Symmetry energy, Relativistic mean field

I. INTRODUCTION

The equation of state (EOS) of nuclear matter, which originates from the interactions between nuclear matter, plays an important role in nuclear physics and astrophysics. Heavy-ion collisions, the properties of nuclei, and neutron stars (NSs) have been widely studied to extract the nuclear EOS. Because nuclear many-body problems are highly nonlinear and the EOS is not a directly observable quantity in experiments, there are still some uncertainties in the EOS despite great efforts [1–6]. For instance, the EOS extracted from the GW170817 event has uncertainties at high nuclear densities [2]. Although the EOS can be extracted from the properties of NSs, the internal composition of NSs is still poorly understood. The core of an NS may contain exotic materials such as hyperons, kaons, pions, and deconfined quark matter [7–12]. Heavy-ion collisions in terrestrial laboratories provide a unique opportunity to study both the EOS and exotic materials.

Collective flows of heavy-ion collisions were proposed in the 1970s and first detected in experiments at Bevalac [13–16]. Because collective flows are associated with nucleon-nucleon interactions, nucleon-nucleon scattering, etc., collective flows have been used to extract the nuclear EOS [1]. Collective flows are also helpful for understanding the phase transition between hadronic and quark matter. Generally, when a phase transition between hadronic and quark matter occurs, the collective flows of heavy-ion collisions indicate a soft EOS [17–21]. In addition, the ratios of the isospin particles in heavy-ion collisions, such as π^-/π^+ , K^0/K^+ , and Σ^-/Σ^+ , are thought to be sensitive to the stiffness of the EOS [22–28]. The production of pions and kaons has been experimentally measured in $^{197}\text{Au}+^{197}\text{Au}$ collisions. The K^+ production predicted by various transport models favors a

soft EOS of isospin-symmetric nuclear matter at high baryon densities [29–33]. The π^-/π^+ ratio predicted by various transport models is still model-dependent [34–37]. Based on the FOPI data for the π^-/π^+ ratio [38], some results favor a stiff symmetry energy (isospin asymmetric part of the EOS) [34, 35], whereas others imply a soft symmetry energy [36, 37]. Recently, by analyzing the ratios of charged pions in $^{132}\text{Sn}+^{124}\text{Sn}$, $^{112}\text{Sn}+^{124}\text{Sn}$, and $^{108}\text{Sn}+^{112}\text{Sn}$ collisions [39], a slope of the symmetry energy ranging from 42 to 117 MeV was suggested [40, 41]. The collective flows and ratios of charged pions are still worth studying to find the sources of the difference in various transport models and to extract information about the EOS from heavy-ion collisions.

Quantum molecular dynamics (QMD) is a popular transport model that has been developed into many versions and used to successfully describe the properties of nuclear matter, nuclei, mesons, and hyperons [33, 34, 42–55]. In high-energy heavy-ion collisions, the relativistic effects should be considered in QMD because they become significant. The RQMD approach has been proposed for this purpose [42, 43]. Recently, relativistic mean field theory (RMF) was implemented in RQMD (RQMD.RMF) [44–46]. The RQMD.RMF has been successfully applied to investigate the collective flows of hadrons [44–46]. In this study, we implemented RMF theory with isovector-vector and isovector-scalar fields in the Lanzhou quantum molecular dynamics model (LQMD.RMF). The channels for the generation and decay of resonances ($\Delta(1232)$, $N^*(1440)$, $N^*(1535)$, etc.), hyperons, and mesons were included in the previous LQMD model [33, 34, 47–50]. Using the LQMD.RMF, we explored the relationship between the symmetry energy and the properties of the collective flow and pion production.

The remainder of this paper is organized as follows. In Sec. II, we briefly introduce the formulas and approaches used in this study. The formulas include RMF theory, the dispersion relation, and the production of pions. The results and discussion are presented in Sec. III. Finally, a summary is presented in Sec. IV.

* This study was supported by the National Natural Science Foundation of China (Nos. 12147106, 12175072, and 11722546) and the Talent Program of South China University of Technology (Project No. 20210115).

† Corresponding author, fengzqh@scut.edu.cn

II. FORMALISM

A. Relativistic mean field approach

The RMF interaction is achieved by exchanging mesons. Scalar and vector mesons provide medium-range attraction and short-range repulsion between nucleons, respectively [56]. The nonlinear self-interaction of the σ meson is introduced to reduce the incompressibility of a reasonable domain [57]. To investigate the properties of symmetry energy, we also consider the isovector-vector ρ [58] and isovector-scalar δ mesons [59]. The Lagrangian density is expressed as [59, 60]

$$\begin{aligned} \mathcal{L} = & \bar{\psi}[\gamma_\mu(i\partial^\mu - g_\omega\omega^\mu - g_\rho\vec{\tau} \cdot \vec{b}^\mu) - (M_N - g_\sigma\sigma \\ & - g_\delta\vec{\tau} \cdot \vec{\delta})]\psi + \frac{1}{2}(\partial_\mu\sigma\partial^\mu\sigma - m_\sigma^2\sigma^2) - \frac{1}{3}g_2\sigma^3 \\ & - \frac{1}{4}g_3\sigma^4 + \frac{1}{2}m_\omega^2\omega_\mu\omega^\mu - \frac{1}{4}F_{\mu\nu}F^{\mu\nu} + \frac{1}{2}m_\rho^2\vec{b}_\mu\vec{b}^\mu \\ & - \frac{1}{4}\vec{B}_{\mu\nu}\vec{B}^{\mu\nu} + \frac{1}{2}(\partial_\mu\vec{\delta} \cdot \partial^\mu\vec{\delta} - m_\delta^2\vec{\delta}^2), \end{aligned} \quad (1)$$

where $M_N = 938$ MeV is the nucleon mass in free space, g_i with $i = \sigma, \omega, \rho, \delta$ is the coupling constant between nucleons, m_i with $i = \sigma, \omega, \rho, \delta$ denotes the meson mass, g_2 and g_3 are the coupling constants for the nonlinear self-interaction of the σ meson, and $F_{\mu\nu} = \partial_\mu\omega_\nu - \partial_\nu\omega_\mu$ and $\vec{B}_{\mu\nu} = \partial_\mu\vec{b}_\nu - \partial_\nu\vec{b}_\mu$ are the strength tensors of the ω and ρ mesons, respectively. The equations of motion for the nucleon and meson are obtained from the Euler-Lagrange equations and are written as:

$$[i\gamma^\mu\partial_\mu - g_\omega\gamma^0\omega_0 - g_\rho\gamma^0\vec{b}_0\vec{\tau}_3 - (M_N - g_\sigma\sigma - g_\delta\tau_3\delta_3)]\psi = 0 \quad (2)$$

$$m_\sigma^2\sigma + g_2\sigma^2 + g_3\sigma^3 = g_\sigma\bar{\psi}\psi = g_\sigma\rho_S \quad (3)$$

$$m_\omega^2\omega_0 = g_\omega\bar{\psi}\gamma^0\psi = g_\omega\rho \quad (4)$$

$$m_\rho^2\vec{b}_0 = g_\rho\bar{\psi}\gamma^0\vec{\tau}_3\psi = g_\rho\rho_3, \quad (5)$$

$$m_\delta^2\delta_3 = g_\delta\bar{\psi}\tau_3\psi = g_\delta\rho_{S3}, \quad (6)$$

where ρ and ρ_S are the baryon and scalar densities, respectively, $\rho_3 = \rho_p - \rho_n$ is the difference between the proton and neutron densities, and $\rho_{S3} = \rho_{Sp} - \rho_{Sn}$ is the difference between the proton and neutron scalar densities.

In the RMF approximation, the energy density is given by

$$\begin{aligned} \epsilon = & \sum_{i=n,p} 2 \int_0^{p_F} \frac{d^3p}{(2\pi)^3} \sqrt{p^2 + M_i^{*2}} + \frac{1}{2}m_\sigma^2\sigma^2 + \frac{1}{3}g_2\sigma^3 \\ & + \frac{1}{4}g_3\sigma^4 + \frac{1}{2}m_\omega^2\omega_0^2 + \frac{1}{2}m_\rho^2\vec{b}_0^2 + \frac{1}{2}m_\delta^2\delta_3^2, \end{aligned} \quad (7)$$

where p_F denotes the nucleon Fermi momentum, and $M_i^* = M_N - g_\sigma\sigma \mp g_\delta\delta_3$ ($-$ proton, $+$ neutron) denotes the effective nucleon mass. The isospin splitting of the effective nucleon mass $M_n^* - M_p^*$ still has a large uncertainty at this point. Analyses of nucleon-nucleus scattering data based on the optical model favor $M_n^* - M_p^* > 0$ [61, 62]. Calculations based on Brueckner theory [63–65] and density-dependent relativistic Hartree-Fock [66] also indicate $M_n^* - M_p^* > 0$. However, $M_n^* - M_p^* < 0$ is predicted by the transport model for heavy-ion collisions [67, 68] and nonlinear RMF models [59, 60, 69]. In addition, both $M_n^* - M_p^* < 0$ and $M_n^* - M_p^* > 0$ can be predicted by the point-coupling RMF [69] and Skyrme and Gogny forces [70–76]. Because the Lagrangian density in this study is the same as that in Ref. [59] and [60] except for the parameter settings, as shown in Fig. 1, the negative isospin splitting of the effective nucleon mass $M_n^* - M_p^* < 0$ is consistent with that in Ref. [59] and [60]. In the nonlinear RMF model, the isospin splitting of the effective nucleon mass is primarily determined by the coupling strength of the δ meson. The large coupling strength of the δ meson results in large isospin splitting of the effective nucleon mass. When the coupling strength of the δ meson is zero (set1), there is no isospin splitting of the effective nucleon mass.

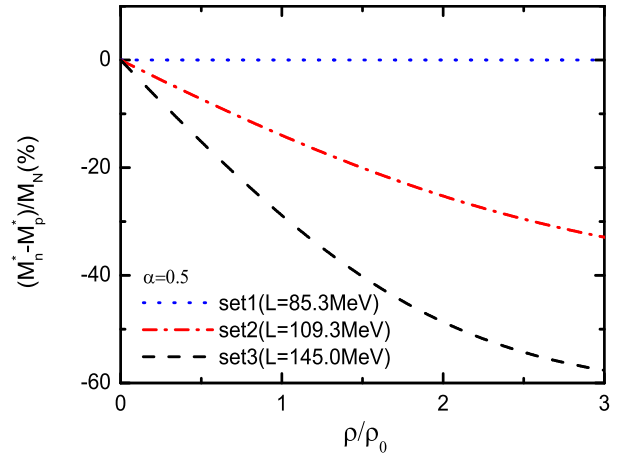


Fig. 1. (Color online) Difference between neutron and proton effective masses as a function of the baryon density.

Using the isospin asymmetry parameter $\alpha = (\rho_n - \rho_p)/(\rho_n + \rho_p)$, the symmetry energy can be written as [59]

$$\begin{aligned} E_{sym} = & \frac{1}{2} \frac{\partial^2 E(\rho, \alpha)}{\partial \alpha^2} \Big|_{\alpha=0} = \frac{1}{2} \frac{\partial^2 [\epsilon(\rho, \alpha)/\rho]}{\partial \alpha^2} \Big|_{\alpha=0} \\ = & \frac{1}{6} \frac{p_F^2}{E_F^*} + \frac{1}{2} f_\rho \rho - \frac{f_\delta}{2} \frac{M^{*2} \rho}{E_F^{*2} [1 + f_\delta A(p_F, M^*)]}, \end{aligned} \quad (8)$$

where $f_i \equiv \frac{g_i^2}{m_i^2}$, $i = \rho, \delta$, and $E_F^* = \sqrt{p_F^2 + M^{*2}}$ and $M^* = M_N - g_\sigma\sigma$ are the effective nucleon masses of the symmetric

144 nuclear matter. The integral $A(p_F, M^*)$ is defined as

$$145 \quad A(p_F, M^*) = \frac{4}{(2\pi)^3} \int d^3p \frac{p^2}{(p^2 + M^{*2})^{3/2}} \\ 146 \quad = 3\left(\frac{\rho_S}{M^*} - \frac{\rho}{E_F^*}\right). \quad (9)$$

147 Based on the symmetry energy E_{sym} , the slope L and curva-
148 ture K_{sym} of the symmetry energy at the saturation density
149 ρ_0 can be obtained as

$$150 \quad L = 3\rho_0 \left(\frac{\partial E_{sym}}{\partial \rho} \right) \Big|_{\rho=\rho_0} \\ 151 \quad K_{sym} = 9\rho_0^2 \left(\frac{\partial^2 E_{sym}}{\partial \rho^2} \right) \Big|_{\rho=\rho_0}. \quad (10)$$

152 In this study, we set the saturation density to $\rho_0 =$
153 $0.16 fm^{-3}$, and the binding energy per particle of the sym-
154 metric nuclear matter was set to $E/A - M_N = -16$ MeV. For
155 symmetric nuclear matter, we set set1, set2, and set3 models
156 to be the same as the result of vanishing isospin asymme-
157 try. As shown in Table 1 and Fig. 2, the symmetry energy
158 of set1, set2, and set3 was set to be 31.6 MeV at the satu-
159 ration density. Set1 contained only ρ mesons; however, set2
160 and set3 contained both the ρ and δ mesons. For set1, when
161 the symmetry energy was set to be 31.6 MeV at the saturation
162 density, the coupling parameter g_ρ was fixed and the slope
163 of symmetry was fixed at $L = 85.3$ MeV. For set2 and set3,
164 when the symmetry energy was fixed at 31.6 MeV, the slope
165 of the symmetry energy was obtained by varying the coupling
166 parameters g_ρ and g_δ . Because the effective mass M^* of the
167 above models for symmetric nuclear matter was the same, the
168 symmetry energy with both the ρ and δ mesons could not be
169 softer than that of set1 containing only ρ mesons. To broaden
170 the range of the slope parameters, we set the slope param-
171 eter of set2 and set3 to be 109.3 and 145.0 MeV by varying
172 the coupling parameters g_ρ and g_δ , respectively. A broader
173 range of slope parameters would be helpful for understanding
174 the relationship between the properties of symmetry energy
175 and the observables of heavy-ion collisions. The curvature
176 of the symmetry energy K_{sym} , which is a higher-order expan-
177 sion coefficient of the symmetry energy compared to the slope
178 parameter L , may also affect the properties of the symmetry
179 energy and the observables of heavy-ion collisions at densi-
180 ties far beyond the saturation density. K_{sym} of set1, set2, and
181 set3 is obtained as -15, 141, and 391 MeV, respectively.

182 B. Relativistic quantum molecular dynamics approach

183 To investigate high-energy heavy-ion collisions, RQMD
184 was proposed [42, 43]. Recently, RMF was implemented in
185 RQMD [44–46]. In RQMD, for an N -body system, there
186 are $4N$ position coordinates q_i^μ and $4N$ momentum coordi-
187 nates p_i^μ ($i = 1, \dots, N$). However, the physical trajectories
188 (\vec{q}_i and \vec{p}_i) are $6N$ for an N -body system. $2N$ constraints
189 are required to reduce the number of dimensions from $8N$ to
190 physical trajectories $6N$ [42–46, 77–79].

$$191 \quad \phi_i \approx 0 (i = 1, \dots, 2N), \quad (11)$$

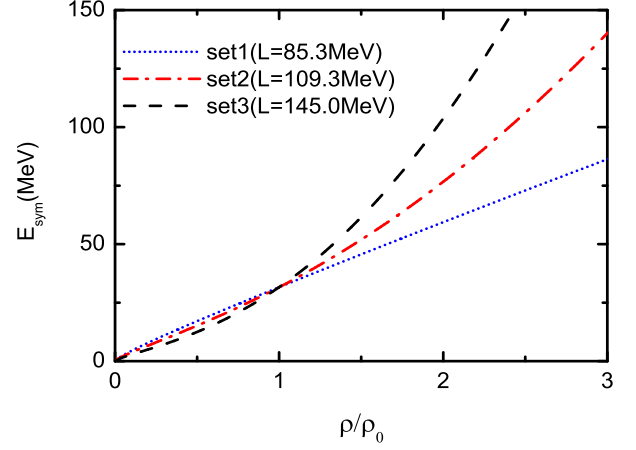


Fig. 2. (Color online) Symmetry energy as a function of the baryon density.

192 where $2N$ constraints satisfy the physical $6N$ phase space.
193 The sign \approx indicates Dirac's weak equality. The on-mass
194 shell conditions can reduce the phase space from $8N$ to $7N$
195 dimensions.

$$196 \quad \phi_i \equiv p_i^{*2} - M_i^{*2} = (p_i - V_i)^2 - (M_N - S_i)^2 = 0, \quad (12)$$

197 where $i = 1, \dots, N$. The remaining N constraints are time fix-
198 ation constraints. A simple choice of time fixation constraints
199 that obey the worldline condition is written as [43, 77, 79, 80]

$$200 \quad \phi_{i+N} \equiv \hat{a} \cdot (q_i - q_N) = 0, (i = 1, \dots, N-1), \\ 201 \quad \phi_{2N} \equiv \hat{a} \cdot q_N - \tau = 0, \quad (13)$$

202 where $\hat{a} = (1, \vec{0})$ denotes a four-dimensional unit-vector [42–
203 46, 77]. In a two-body center-of-mass system, \hat{a} is defined as
204 $p_{ij}^\mu / \sqrt{p_{ij}^2}$ with $p_{ij}^\mu = p_i^\mu + p_j^\mu$. We observe that only the con-
205 straint $i = 2N$ depends on τ . With the above $2N$ constraints,
206 the number of dimensions from $8N$ will reduce to $6N$. These
207 $2N$ constraints are conserved over time.

$$208 \quad \frac{d\phi_i}{d\tau} = \frac{\partial \phi_i}{\partial \tau} + \sum_k C_{ik}^{-1} \lambda_k = 0. \quad (14)$$

209 Because only the constraint $i = 2N$ depends on τ , λ is writ-
210 ten as [77]

$$211 \quad \lambda_i = -C_{2N,i} \frac{\partial \phi_{2N}}{\partial \tau}, (i = 1, \dots, 2N-1), \quad (15)$$

212 with $C_{ij}^{-1} = [\phi_i, \phi_j]$. Following previous studies, the Hamil-
213 tonian of the N -body system was constructed as a linear com-
214 bination of $2N-1$ constraints [77, 79, 80]:

$$215 \quad H = \sum_{i=1}^{2N-1} \lambda_i(\tau) \phi_i, \quad (16)$$

Table 1. Parameter sets for RMF. The saturation density ρ_0 is set to 0.16 fm^{-3} . The binding energy of the saturation density is $E/A - M_N = -16 \text{ MeV}$. The isoscalar-vector ω and isovector-vector ρ masses are fixed at their physical values, $m_\omega = 783 \text{ MeV}$ and $m_\rho = 763 \text{ MeV}$, respectively. The remaining meson masses, m_σ and m_δ , are set to be 550 and 500 MeV, respectively.

model	g_σ	g_ω	$g_2 (\text{fm}^{-1})$	g_3	g_ρ	g_δ	$K (\text{MeV})$	$E_{\text{sym}}(\rho_0) (\text{MeV})$	$L(\rho_0) (\text{MeV})$	$M^*(\rho_0)/M_N$	$K_{\text{sym}} (\text{MeV})$
set1	8.145	7.570	31.820	28.100	4.049	-	230	31.6	85.3	0.81	-15
set2	8.145	7.570	31.820	28.100	8.673	5.347	230	31.6	109.3	0.81	141
set3	8.145	7.570	31.820	28.100	11.768	7.752	230	31.6	145.0	0.81	391

Assuming $[\phi_i, \phi_j] = 0$, $\lambda_i = 0$ for $N + 1 < i < 2N$ [77].
The equations of motion are then obtained as

$$\begin{aligned} \frac{dq_i}{d\tau} &= [H, q_i] = \sum_j^N \lambda_j \frac{\partial \phi_j}{\partial p_i}, \\ \frac{dp_i}{d\tau} &= [H, p_i] = - \sum_j^N \lambda_j \frac{\partial \phi_j}{\partial q_i}, \end{aligned} \quad (17)$$

with the on-mass shell conditions (Eq. (12)) as inputs, the equations of motion can be obtained as

$$\begin{aligned} \dot{\vec{r}}_i &= \frac{\vec{p}_i^*}{p_i^{*0}} + \sum_{j=1}^N \left(\frac{M_j^*}{p_j^{*0}} \frac{\partial M_j^*}{\partial \vec{p}_i} + z_j^{*\mu} \cdot \frac{\partial V_{j\mu}}{\partial \vec{p}_i} \right), \\ \dot{\vec{p}}_i &= - \sum_{j=1}^N \left(\frac{M_j^*}{p_j^{*0}} \frac{\partial M_j^*}{\partial \vec{r}_i} + z_j^{*\mu} \cdot \frac{\partial V_{j\mu}}{\partial \vec{r}_i} \right), \end{aligned} \quad (18)$$

where $z_i^{*\mu} = p_i^{*\mu}/p_i^{*0}$ and $M_i^* = M_N - S_i$. The scalar potential S_i and vector potential $V_{i\mu}$ in RQMD are defined as

$$\begin{aligned} S_i &= g_\sigma \sigma_i + g_\delta t_i \delta_i, \\ V_{i,\mu} &= B_i g_\omega \omega_{i,\mu} + B_i t_i g_\rho b_{i,\mu}, \end{aligned} \quad (19)$$

where $t_i = 1$ for protons, and $t_i = -1$ for neutrons, and B_i is the baryon number of the i th particle. The meson field can be obtained from the RMF:

$$\begin{aligned} m_\sigma^2 \sigma_i + g_2 \sigma_i^2 + g_3 \sigma_i^3 &= g_\sigma \rho_{S,i}, \\ m_\omega^2 \omega_i^\mu &= g_\omega J_i^\mu, \\ m_\delta^2 \delta_i &= g_\delta (\rho_{Sp,i} - \rho_{Sn,i}) = g_\delta \rho_{S3,i}, \\ m_\rho^2 b_i^\mu &= g_\rho (\rho_{p,i} - \rho_{n,i}) = g_\rho R_i^\mu. \end{aligned} \quad (20)$$

Substituting Eq. (20) into Eq. (19), the scalar potential S_i and vector potential $V_{i\mu}$ of the nucleons can be obtained. For other hadrons, such as Δ resonances, similar to other transport models [34, 85], the Δ optical potential is estimated using the nucleon potentials and square of the Clebsch–Gordan coefficient. In the RQMD approach, the scalar density, isovector-scalar density, baryon current, and isovector baryon current are expressed as

$$\begin{aligned} \rho_{S,i} &= \sum_{j \neq i} \frac{M_j}{p_j^0} \rho_{ij}, & \rho_{S3,i} &= \sum_{j \neq i} t_j \frac{M_j}{p_j^0} \rho_{ij}, \\ J_i^\mu &= \sum_{j \neq i} B_j \frac{p_j^\mu}{p_j^0} \rho_{ij}, & R_i^\mu &= \sum_{j \neq i} t_j B_j \frac{p_j^\mu}{p_j^0} \rho_{ij}. \end{aligned} \quad (21)$$

Because the difference between the numerical results obtained using the effective mass M_j^* and kinetic momentum $p_j^{\mu*}$ in the density and current and those obtained using a free mass $M_j = M_N = 938 \text{ MeV}$ and canonical momentum p_j^μ in the density and current is small, a free mass $M_j = M_N = 938 \text{ MeV}$ and canonical momentum p_j^μ have been used in the above density and current [45]. The interaction density ρ_{ij} is given by a Gaussian

$$\rho_{ij} = \frac{\gamma_{ij}}{(4\pi L_G)^{3/2}} \exp\left(\frac{q_{T,ij}^2}{4L_G}\right), \quad (22)$$

where $q_{T,ij}^2 = q_{ij}^2 - [\frac{q_{ij,\sigma}(p_i^\sigma + p_j^\sigma)}{\sqrt{(p_i + p_j)^2}}]^2$ is a distance squared [77], and γ_{ij} is a Lorentz factor that ensures the correct normalization of the Gaussian [81] and is equal to $(p_i^0 + p_j^0)/(p_i + p_j)$ in the two-body center-of-mass frame. In this study, we set the Gaussian width to $L_G = 2.0 \text{ fm}^2$.

C. Dispersion relation and production of pions

The Hamiltonian of the mesons is defined as [48, 82–84]

$$H_M = \sum_{i=1}^{N_M} [V_i^C + \omega(\vec{p}_i, \rho_i)], \quad (23)$$

where V_i^C is the Coulomb potential, which is expressed as

$$V_i^C = \sum_{j=1}^{N_B} \frac{e_i e_j}{r_{ij}}, \quad (24)$$

and N_M and N_B are the total numbers of mesons and baryons, including charged resonances, respectively. The pion potential in the medium, which contains isoscalar and isovector contributions, is defined as

$$\omega(\vec{p}_i, \rho_i) = \omega_{\text{isoscalar}}(\vec{p}_i, \rho_i) + C_\pi \tau_z \alpha (\rho/\rho_0)^{\gamma_\pi}, \quad (25)$$

where α denotes the isospin asymmetry parameter, the coefficient C_π is 36 MeV, the isospin quantity τ is 1, 0, and -1 for π^- , π^0 , and π^+ , respectively, and γ_π determines the isospin splitting of the pion potential and is set to two. In this study, the isoscalar part of pion potential $\omega_{\text{isoscalar}}$ was chosen as the Δ -hole model. The pion potential, which contains a pion branch (smaller value) and Δ -hole (larger value) branch, is defined as

$$\begin{aligned} \omega_{\text{isoscalar}}(\vec{p}_i, \rho_i) &= S_\pi(\vec{p}_i, \rho_i) \omega_{\pi\text{-like}}(\vec{p}_i, \rho_i) + \\ &S_\Delta(\vec{p}_i, \rho_i) \omega_{\Delta\text{-like}}(\vec{p}_i, \rho_i). \end{aligned} \quad (26)$$

The probabilities of the pion and Δ -hole branches satisfy the following equation:

$$S_\pi(\vec{p}_i, \rho_i) + S_\Delta(\vec{p}_i, \rho_i) = 1. \quad (27)$$

The probability of both the pion and Δ -hole branches is defined as [84]

$$S(\vec{p}_i, \rho_i) = \frac{1}{1 - \partial\Pi(\omega)/\partial\omega^2}, \quad (28)$$

where ω denotes $\omega_{\pi-like}$ and $\omega_{\Delta-like}$. The eigenvalues of $\omega_{\pi-like}$ and $\omega_{\Delta-like}$ are generated from the pion dispersion relation

$$\omega^2 = \vec{p}_i^2 + m_\pi^2 + \Pi(\omega), \quad (29)$$

where Π denotes the pion self-energy. Including the short-range Δ -hole interaction, the pion self-energy is defined as

$$\Pi = \frac{\vec{p}_i^2 \chi}{1 - g' \chi}, \quad (30)$$

where m_π denotes pion mass. The Migdal parameter, g' , was set to 0.6. χ is defined as

$$\chi = -\frac{8}{9} \left(\frac{f_\Delta}{m_\pi} \right)^2 \frac{\omega_\Delta \rho \hbar^3}{\omega_\Delta^2 - \omega^2} \exp(-2\vec{p}_i^2/b^2), \quad (31)$$

where $\omega_\Delta = \sqrt{m_\Delta^2 + \vec{p}_i^2} - M_N$ and m_Δ is the delta mass. In this study, the $\pi N \Delta$ coupling constant f_Δ was 2, and the cutoff factor b was $7m_\pi$.

Both the Coulomb and pion potentials contribute to the decay of resonances and the reabsorption of pions. For instance, the energy balance of Δ^0 in the decay of resonances and the reabsorption of pions can be written as

$$\sqrt{m_R^2 + \vec{p}_R^2} = \sqrt{M_N^2 + (\vec{p}_R - \vec{p}_\pi)^2} + \omega_\pi(\vec{p}_\pi, \rho) + V_\pi^C, \quad (32)$$

where \vec{p}_R and \vec{p}_π are the momenta of the resonances and pions, respectively, and m_R is the mass of the resonances. Because Δ^0 is uncharged, the Coulomb potential exists only for charged particles after the decay of Δ^0 .

The pion is generated from direct nucleon-nucleon collision and decay of the resonances $\Delta(1232)$ and $N^*(1440)$. The reaction channels of the resonances and pions, which are the same as those in the LQMD model, are as follows [33, 48, 88, 89]:

$$\begin{aligned} NN &\leftrightarrow N\Delta, \quad NN \leftrightarrow NN^*, \quad NN \leftrightarrow \Delta\Delta, \quad \Delta \leftrightarrow N\pi, \\ N^* &\leftrightarrow N\pi, \quad NN \rightarrow NN\pi(s\text{-state}). \end{aligned} \quad (33)$$

For the production of the $\Delta(1232)$ and $N^*(1440)$ resonances in nucleon-nucleon scattering, the parameterized cross-sections calculated using the one-boson exchange model were employed [91].

The decay width of $\Delta(1232)$ and $N^*(1440)$, which originates from the p-wave resonances, is momentum-dependent and is expressed as [91]

$$\Gamma(|\vec{p}|) = \frac{a_1 |\vec{p}|^3}{(1 + a_2 |\vec{p}|^2)(a_3 + |\vec{p}|^2)} \Gamma_0, \quad (34)$$

where $|\vec{p}|$ is the momentum of the created pion (in GeV/c). The parameters a_1 , a_2 , and a_3 were taken as 22.48 (17.22) c/GeV , 39.69 (39.69) c^2/GeV^2 , and 0.04(0.09) GeV^2/c^2 , respectively, for $\Delta(N^*)$. The bare decay width of $\Delta(N^*)$ was given by $\Gamma_0 = 0.12(0.2)\text{GeV}$. With the momentum-dependent decay width, the cross-section of pion-nucleon scattering has the Breit-Wigner form:

$$\sigma_{\pi N}(\sqrt{s}) = \sigma_{\max} \left(\frac{\vec{p}_m}{\vec{p}} \right)^2 \frac{0.25\Gamma^2(\vec{p})}{0.25\Gamma^2(\vec{p}) + (\sqrt{s} - m_0)^2}, \quad (35)$$

where \vec{p} and \vec{p}_m are the three momenta of the pions at energies of \sqrt{s} and m_0 , respectively. The maximum cross-section σ_{\max} of Δ and N^* resonances was obtained by fitting the total cross-sections of the experimental data in pion-nucleon scattering using the Breit-Wigner formula [92]. For instance, the maximum cross-section σ_{\max} of Δ resonance was 200, 133.33, and 66.7 mb for $\pi^+p \rightarrow \Delta^{++}$ ($\pi^-n \rightarrow \Delta^-$), $\pi^0p \rightarrow \Delta^+$ ($\pi^0n \rightarrow \Delta^0$) and $\pi^-p \rightarrow \Delta^0$ ($\pi^+n \rightarrow \Delta^+$), respectively [89].

Note that the threshold effect was neglected in this study. The threshold effect mainly refers to the Δ production threshold energy and incident energy of two colliding nucleons modified by the medium. The incident and threshold energies in the medium are defined

$$\text{as } \sqrt{s_{in}} = \sqrt{(E_1^* + \Sigma_1^0 + E_2^* + \Sigma_2^0)^2 - (\vec{\Sigma}_1 + \vec{\Sigma}_2)^2} \text{ and}$$

$$\sqrt{s_{th}} = \sqrt{(m_3^* + \Sigma_3^0 + m_4^* + \Sigma_4^0)^2 - (\vec{\Sigma}_3 + \vec{\Sigma}_4)^2}, \text{ respec-}$$

tively [85–87]. Because $\vec{\Sigma}_i = 0$ and $\vec{p}_i^* \simeq 0$ for static nuclear matter, the difference between the incident and threshold energies is $\sqrt{s_{in}} - \sqrt{s_{th}} = E_1^* + \Sigma_1^0 + E_2^* + \Sigma_2^0 - m_3^* - \Sigma_3^0 - m_4^* - \Sigma_4^0$ [86]. The difference between the incident and threshold energies, which is isospin dependent, may result in an enhancement in the $nn \rightarrow p\Delta^-$ channel and suppression of the $pp \rightarrow n\Delta^{++}$ channel.

III. RESULTS AND DISCUSSIONS

The directed and elliptic flows were derived from the Fourier expansion of the azimuthal distribution:

$$\begin{aligned} \frac{dN}{d\phi}(y, p_T) = N_0 [1 + 2V_1(y, p_T)\cos(\phi) \\ + 2V_2(y, p_T)\cos(2\phi)], \end{aligned} \quad (36)$$

where the azimuthal angle of the emitted particle ϕ was measured from the reaction plane. $p_T = \sqrt{p_x^2 + p_y^2}$ denotes the transverse momentum, and the directed flow V_1 and elliptic flow V_2 are expressed as follows:

$$\begin{aligned} V_1 &\equiv \langle \cos(\phi) \rangle = \langle \frac{p_x}{p_T} \rangle, \\ V_2 &\equiv \langle \cos(2\phi) \rangle = \langle \frac{p_x^2 - p_y^2}{p_T^2} \rangle. \end{aligned} \quad (37)$$

The directed flow provides information on the azimuthal anisotropy of the transverse emission. The elliptic flow describes the competition between the in-plane ($V_2 > 0$) and out-of-plane ($V_2 < 0$) emissions.

Firstly, the collective flows of LQMD.RMF in the $^{197}\text{Au} + ^{197}\text{Au}$ collisions have been investigated at an incident energy of 2.92 GeV/nucleon (the corresponding nucleon-nucleon center-of-mass energy is $\sqrt{S_{NN}} = 3$ GeV). The collective flows of LQMD with Skyrme interaction and without the momentum-dependent interaction have also been investigated. The Skyrme interaction of symmetric nuclear matter is taken to be the same as that of SLy6, with an incompressibility of $K = 230$ MeV at $\rho_0 = 0.16 \text{ fm}^{-3}$ [93, 94]. The symmetry energy of Skyrme interaction is defined as $E_{\text{sym}} = \frac{1}{3} \frac{\hbar^2}{2M_N} (\frac{3\pi^2\rho}{2})^{2/3} + \frac{C_{\text{sym}}}{3} (\rho/\rho_0)^{\gamma_s}$. When the C_{sym} and γ_s are set to be 38.6 MeV and 1.049, respectively, the symmetry energy and the slope parameter of symmetry energy are 31.6 MeV and 85.3 MeV, respectively. The symmetry energy and the slope parameter of symmetry energy of the Skyrme interaction are as same as those of set1. As shown in Fig. 3, we have compared the collective flows of LQMD.RMF and LQMD with Skyrme interaction with recent experimental data from STAR Collaboration [90]. The collective flows of LQMD.RMF and LQMD with Skyrme interaction can describe the STAR data at an impact parameter $b=4$ fm and $b=7$ fm, respectively. The directed flows of LQMD.RMF are almost consistent with the STAR data across the entire rapidity. However, The directed flows of LQMD with Skyrme interaction are weaker than the STAR data across the entire rapidity. This result may be due to the fact that the value of directed transverse momentum with the Lorentz effect is larger than that without the Lorentz effect [43]. The elliptic flows of both LQMD.RMF and LQMD with Skyrme interaction are consistent with the STAR data at rapidities smaller than 0.5. However, the elliptic flows of both LQMD.RMF and LQMD with Skyrme interaction are weaker than the STAR data at large rapidity. At an incident energy of 2.92 GeV/nucleon, the LQMD.RMF can better describe the experimental data compared to the LQMD with Skyrme interaction and without the momentum-dependent interaction. Based on the above analyses, the RMF models have been implemented into the LQMD model successfully.

With this LQMD.RMF model, the $^{108}\text{Sn} + ^{112}\text{Sn}$ and $^{132}\text{Sn} + ^{124}\text{Sn}$ collisions in this study were investigated at an incident energy of 270 A MeV and an impact parameter $b=3$ fm. At an incident energy of 270 A MeV, the nuclear matter of the collision center can be compressed to densities approaching $2\rho_0$. In this dense region, collective flows, which reflect nucleon-nucleon interactions, can be used to extract the high-density behavior of the EOS [1, 44, 79, 88, 95]. The collective flows of free protons in the $^{108}\text{Sn} + ^{112}\text{Sn}$ and $^{132}\text{Sn} + ^{124}\text{Sn}$ collisions are shown in Fig. 4 and Fig. 5, respectively. It is reasonable that the maximum value of the directed flow V_1 was significantly larger than that of the elliptic flow V_2 . In the same reaction system, the difference in the directed flows with various slopes of symmetry energy (set1, set2, and set3) was small. The difference in the elliptic flows with various slopes of symmetry energy was also small. To determine the relationship between the slope of the symmetry energy and the collective flow, we must process the collective flow data. The difference between neutron and proton directed flows emitted from heavy-ion collisions can

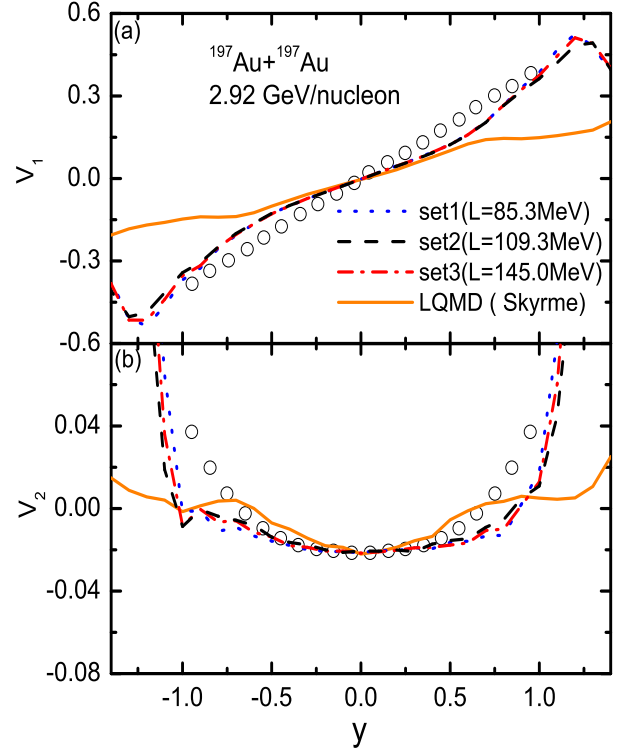


Fig. 3. (Color online) Rapidity distribution of the collective flows of free protons in the $^{197}\text{Au} + ^{197}\text{Au}$ reaction at an incident energy of 2.92 GeV/nucleon. The open circles correspond to the STAR data [90].

be used to extract the density dependence of the symmetry energy [88, 95]. The difference between the neutron and proton directed flows is defined as $V_{1n} - V_{1p}$, as shown in Fig. 6. The trend and shape of the difference between the neutron and proton directed flows were similar to those of nonrelativistic LQMD [88]. For a given reaction system (nearly symmetric $^{108}\text{Sn} + ^{112}\text{Sn}$ system or neutron-rich $^{132}\text{Sn} + ^{124}\text{Sn}$ system), the absolute value of the difference between the neutron and proton directed flows with a soft symmetry energy was higher than that with a stiff symmetry energy. Interestingly, the stiffness of the symmetry energy can be reflected through the difference between the neutron and proton directed flows. The relationship between the curvature of the symmetry energy K_{sym} and the collective flows was then investigated. The difference between K_{sym} of set1 and K_{sym} of set3 was 406 MeV, which was significantly larger than the 59.7 MeV difference between L of set1 and L of set3. Although the curvature of the symmetry energy K_{sym} also affected the difference between the neutron and proton directed flows, because the nuclear matter of the collision center could only approach $2\rho_0$ at an incident energy of 270 A MeV, the effects of K_{sym} were not significant compared to the effects of the slope parameter L .

In addition to collective flows, the production of isospin exotic particles such as hyperons, kaons, and pions can also be used to extract the symmetry energy [22–28]. Because the thresholds of hyperons and kaons were not reached at the in-

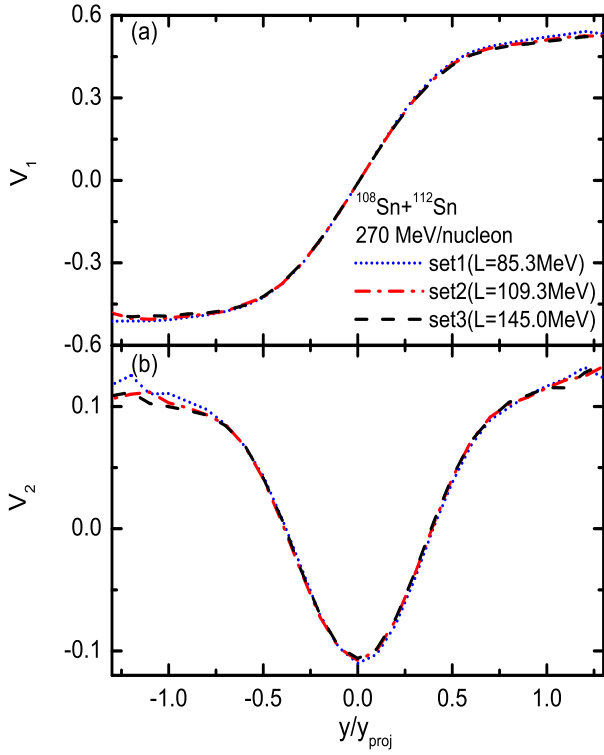


Fig. 4. (Color online) Rapidity distribution of the collective flows of free protons in the $^{108}\text{Sn} + ^{112}\text{Sn}$ reaction at an incident energy of 270 MeV/nucleon.

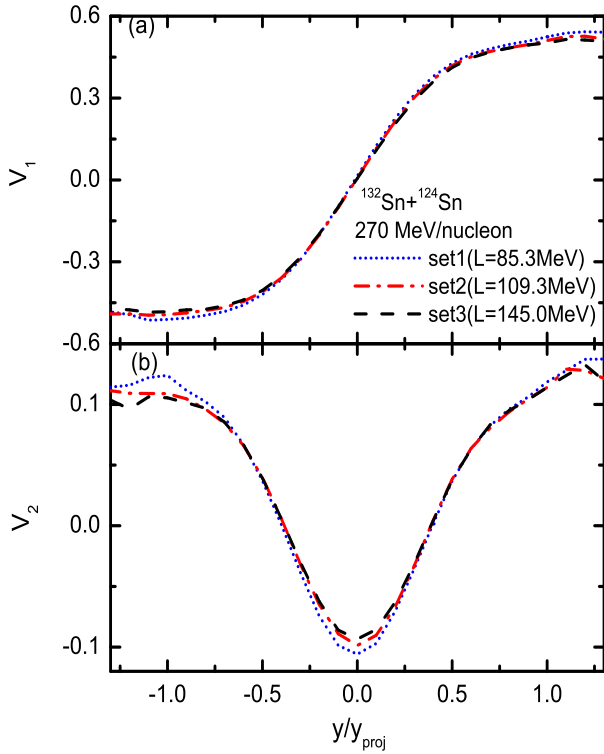


Fig. 5. (Color online) Rapidity distribution of the collective flows of free protons in the $^{132}\text{Sn} + ^{124}\text{Sn}$ reaction at an incident energy of 270 MeV/nucleon.

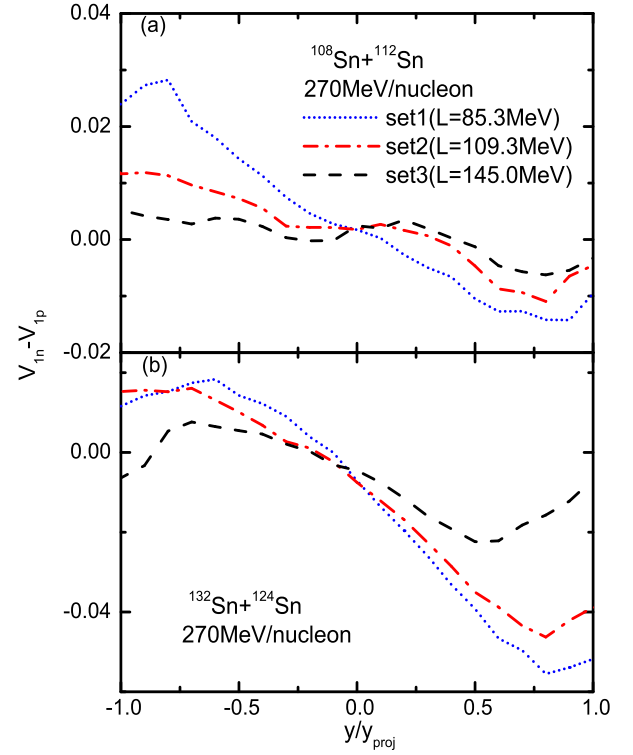


Fig. 6. (Color online) Difference between neutron and proton directed flows in the $^{108}\text{Sn} + ^{112}\text{Sn}$ and $^{132}\text{Sn} + ^{124}\text{Sn}$ reactions at an incident energy of 270 MeV/nucleon.

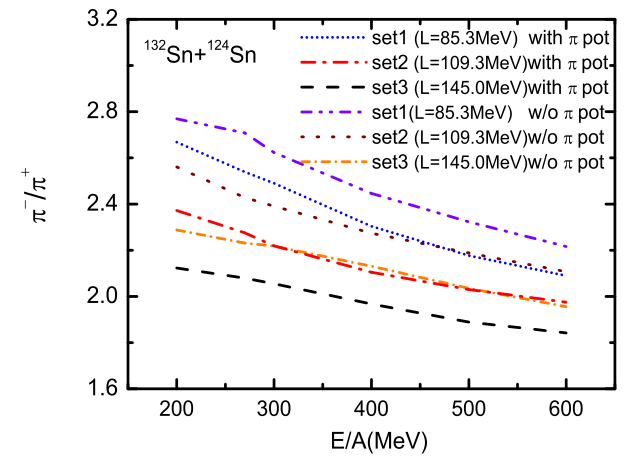


Fig. 7. (Color online) Ratio between the π^- and π^+ yields as a function of the incident energy in the $^{132}\text{Sn} + ^{124}\text{Sn}$ reaction.

458 incident energies in this study, the isospin exotic particles were
 459 pions. First, we calculated the ratio between the π^- and π^+
 460 yields of the neutron-rich $^{132}\text{Sn} + ^{124}\text{Sn}$ system as a func-
 461 tion of the collision energy at the impact parameter $b=3$ fm
 462 and $\theta_{cm} < 90^\circ$. Because set1 had the softest symmetry en-
 463 ergy, it had the highest neutron density. Consequently, there
 464 were more neutron-neutron scatterings in set1, resulting in
 465 the production of more Δ^- and π^- . As shown in Fig. 7, the
 466 π^-/π^+ ratio of set1 was the highest, and the π^-/π^+ ratio

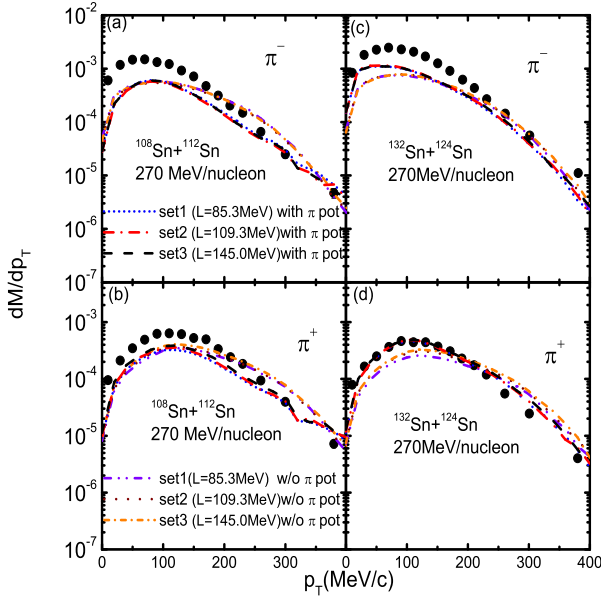


Fig. 8. (Color online) Transverse momentum spectra of pions as functions of transverse momentum at an incident energy of 270 MeV/nucleon. The left two panels [(a) and (b)] are the results of the $^{108}\text{Sn} + ^{112}\text{Sn}$ reaction, and the right two panels [(c) and (d)] are the results of the $^{132}\text{Sn} + ^{124}\text{Sn}$ reaction. The full circles correspond to the S π RIT data [40].

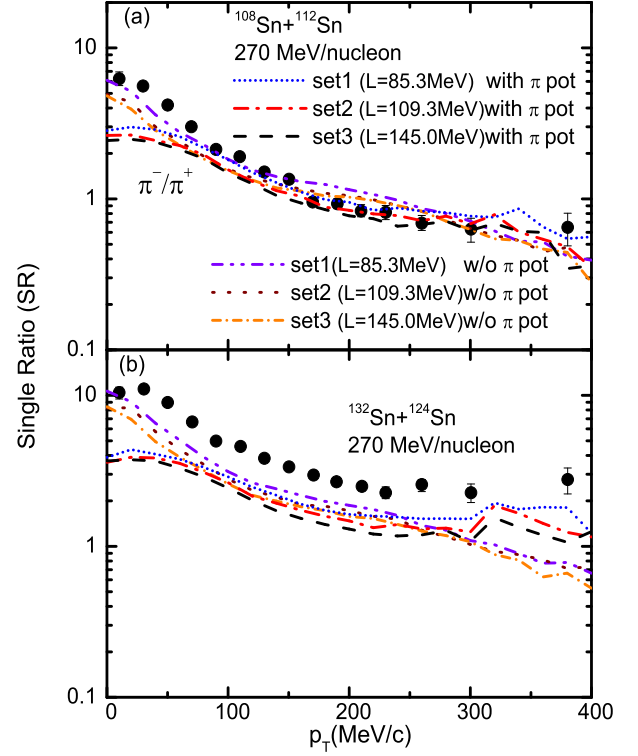


Fig. 9. (Color online) Single spectral ratios of pions as functions of transverse momentum for the $^{108}\text{Sn} + ^{112}\text{Sn}$ and $^{132}\text{Sn} + ^{124}\text{Sn}$ reactions at an incident energy of 270 MeV/nucleon. The full circles correspond to the S π RIT data [40].

of set2 was higher than that of set3. Specifically, at a collision energy of 270 MeV/nucleon, the π^-/π^+ ratio without (with) the π potential changed from 2.71 (2.54) to 2.23 (2.06) when the slope parameter was varied from $L = 85.3$ to 145.0 MeV, that is, from set1 to set3. In other words, the π^-/π^+ ratio as a function of collision energy depends on the stiffness of the symmetry energy. This result was consistent with the predictions of most transport models [28, 39, 86]. When the π potential was considered, the interaction between π and the nucleon became attractive, resulting in a decrease in both π^- and π^+ via the absorbed channels $\pi N \rightarrow \Delta(1232)$ and $\Delta(1232)N \rightarrow NN$. However, with the π potential, because there were more neutrons in the neutron-rich $^{132}\text{Sn} + ^{124}\text{Sn}$ system, π^- was more easily absorbed than π^+ . Consequently, the π^-/π^+ ratio without the π potential was higher than that with the π potential in the same RMF model. Moreover, it is worth mentioning that the threshold effect neglected in this study may cause the π^-/π^+ ratio to be reversed. In other words, with the threshold effect [85–87], π^-/π^+ of set3 may be the highest, and the π^-/π^+ ratio of set2 may be higher than that of set1.

Next, the properties of π were predicted as a function of the transverse momentum. As shown in Fig. 8, the left and right panels are the transverse momentum spectra of pions for the nearly symmetric $^{108}\text{Sn} + ^{112}\text{Sn}$ and neutron rich $^{132}\text{Sn} + ^{124}\text{Sn}$ reactions at $\theta_{cm} < 90^\circ$, respectively. In collisions between isotopes, π^+ is mainly generated from collisions between protons and π^- is mainly generated from collisions between neutrons. Theoretically, a stiffer symmetry energy would have a stronger repulsive force to push out neu-

trons and a stronger attractive force to squeeze protons, resulting in a decrease in the π^- yield and an increase in the π^+ yield, respectively. As shown in panels (b) and (d) of Fig. 8, the stiffer symmetry energy indeed led to larger transverse momentum spectra for π^+ . However, the relationship between the transverse momentum spectra of π^- and the stiffness of the symmetry energy could not be directly explained. Compared with the stiffness of the symmetry energy, the π potential had a more significant impact on the transverse momentum spectrum of π . For the neutron-rich $^{132}\text{Sn} + ^{124}\text{Sn}$ system, the transverse momentum spectra of both π^+ and π^- without the π potential were lower than those of the S π RIT data at $p_T \lesssim 200$ MeV. When the π potential was considered, the transverse momentum spectra of both π^+ and π^- increased at $p_T \lesssim 200$ MeV but decreased at $p_T \gtrsim 200$ MeV. Consequently, the transverse momentum spectra of π^+ with the π potential were almost consistent with the S π RIT data [40]; however, the transverse momentum spectra of π^- were still lower than the S π RIT data for the entire p_T domain. The lower transverse momentum spectra of π^- may be due to the absence of a threshold effect. The threshold effect, which was not considered in this study, may enhance the production of π^- [85–87].

Because a stiffer symmetry energy would have a stronger repulsive force to push out neutrons and a stronger attractive force to squeeze protons, resulting in a decrease in the π^- yield and an increase in the π^+ yield, respectively, the single

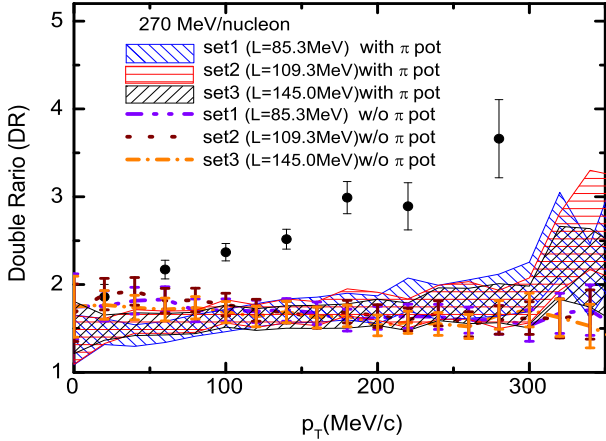


Fig. 10. (Color online) Double ratio of pions as a function of transverse momentum at an incident energy of 270 MeV/nucleon. The full circles correspond to the $S\pi$ RIT data [40].

ratio $SR(\pi^-/\pi^+) = [dM(\pi^-)/dp_T]/[dM(\pi^+)/dp_T]$ may depend on the stiffness of the symmetry energy and the reaction system. As shown in Fig. 9, for both the nearly symmetric system and neutron-rich system, a softer symmetry energy led to a larger single ratio. In addition, for the same stiffness of the symmetry energy, because the neutron-neutron scattering of the neutron-rich $^{132}\text{Sn} + ^{124}\text{Sn}$ system was greater than that of the nearly symmetric $^{108}\text{Sn} + ^{112}\text{Sn}$ system, the single ratio of the neutron-rich system was higher than that of the nearly symmetric system. It is worth mentioning that the single ratio of $^{108}\text{Sn} + ^{112}\text{Sn}$ was almost consistent with the experimental data. However, the single ratio of $^{132}\text{Sn} + ^{124}\text{Sn}$ was lower than that of the experimental data for the entire p_T domain. This was because the transverse momentum spectra π^- of $^{132}\text{Sn} + ^{124}\text{Sn}$ were lower than the experimental data.

The double ratio between the neutron rich system and the nearly symmetric system $DR(\pi^-/\pi^+) = SR(\pi^-/\pi^+)_{132+124}/SR(\pi^-/\pi^+)_{108+112}$, which can cancel out most of the systematic errors caused by Coulomb and isoscalar interactions, was suggested to extract the properties of the symmetry energy [40]. However, because a lower symmetry energy will lead to a larger single ratio for both the nearly symmetric system and neutron-rich system, as shown in Fig. 10, it is still difficult to understand the dependence of the double ratio on the stiffness of symmetry energy. In addition, the double ratio without the π potential decreased slightly as a function of the transverse momentum, whereas it increased slightly as the transverse momentum increased when the π potential was considered. However, the increasing trend was still considerably weaker than that of the experimental results. The lower double ratio originated from the lower single ratio of the neutron-rich $^{132}\text{Sn} + ^{124}\text{Sn}$ system compared with the experimental data. The threshold effect may enhance the production of π^- [85–87] and the single ratio of the neutron-rich system, resulting in a larger double ratio.

IV. CONCLUSION

An RMF with various symmetry energies, namely set1, set2, and set3, was implemented in LQMD. The collective flows of the nearly symmetric $^{108}\text{Sn} + ^{112}\text{Sn}$ and neutron-rich $^{132}\text{Sn} + ^{124}\text{Sn}$ systems were successfully generated from the LQMD.RMF. It has been observed that the directed flow V_1 was an order of magnitude larger than the elliptic flow V_2 . However, the difference between the directed flows V_1 with various slopes of symmetry energy was small. The difference in the directed flows V_2 with various slopes of symmetry energy was also small. To explore the relationship between the collective flow and the stiffness of the symmetry energy, we defined the difference between neutron and proton directed flows $V_{1n} - V_{1p}$. For a given nearly symmetric system or neutron-rich system, the absolute value of $V_{1n} - V_{1p}$ increased with decreasing slope of the symmetry energy.

We also investigated the relationship between isospin exotic particles and the stiffness of the symmetry energy. The ratio between π^- yield and π^+ yield of the neutron-rich $^{132}\text{Sn} + ^{124}\text{Sn}$ system as a function of the collision energy increased with a decrease in the slope parameter of the symmetry energy. At an incident energy of 270 MeV/nucleon, the properties of π were predicted as a function of the transverse momentum. For the nearly symmetric $^{108}\text{Sn} + ^{112}\text{Sn}$ system, the single ratio of the nearly symmetric system was consistent with the experimental data. However, for the neutron-rich $^{132}\text{Sn} + ^{124}\text{Sn}$ system, the single ratio was lower than the experimental data, resulting in a double ratio lower than the experimental data. The π potential did not explain the lower transverse momentum spectra of π^- in the neutron-rich system. Considering the π potential, the double ratio increased slightly with increasing transverse momentum. However, the increasing trend was still considerably weaker than that observed in the experimental results. The single ratio of the neutron-rich system and the double ratio may be lower than the experimental data because of the lack of a threshold effect. The threshold effect, which can enhance the production of π^- , could be a candidate for enhancing the single ratio of the neutron-rich system to a double ratio. Moreover, because a softer symmetry energy led to a larger single ratio for both nearly symmetric and neutron-rich systems, the dependence of the double ratio on the stiffness of the symmetry energy was not significant. The sensitivity of the double ratio to the stiffness of the symmetry energy may also be due to the lack of a threshold effect. When the threshold effect is considered, the production of π^- in a neutron-rich system may be more significant than that in a nearly symmetric system. In the future, when collective flows occur, and the single ratio of the neutron-rich system and the double ratio of the LQMD.RMF are consistent with the experimental data, $V_{1n} - V_{1p}$ and the single ratio of the neutron-rich system π^-/π^+ , which are sensitive to the stiffness of the symmetry energy, may be used to extract the slope parameter of the symmetry energy.

Appendix A: DETAILS of EQUATION OF MOTION

For numerical calculations, the equation of motion (Eq. (18)) must be written in the computed form. With Eq. (19) and $M_i^* = M_i - S_i = M_N - S_i$ as the inputs, the equation of motion (Eq. (18)) can be expanded as

$$\begin{aligned} \vec{r}_i = \frac{\vec{p}_i^*}{p_i^{*0}} + \sum_{j \neq i} [D_{ij} \frac{\partial \rho_{ij}}{\partial \vec{p}_i} + D_{ji} \frac{\partial \rho_{ji}}{\partial \vec{p}_i} \\ + (D_j \frac{\partial f_i}{\partial \vec{p}_i} + A_{ji}^\mu \frac{\partial z_{i\mu}}{\partial \vec{p}_i}) \rho_{ji} \\ + (D_j' t_i \frac{\partial f_i}{\partial \vec{p}_i} + A_{ji}'^\mu \frac{\partial z_{i\mu}}{\partial \vec{p}_i}) \rho_{ji}], \end{aligned} \quad (\text{A1})$$

$$\vec{p} = - \sum_{j \neq i} [D_{ij} \frac{\partial \rho_{ij}}{\partial \vec{r}_i} + D_{ji} \frac{\partial \rho_{ji}}{\partial \vec{r}_i}], \quad (\text{A2})$$

with

$$D_{ij} = D_i f_j + A_{ij}^\mu z_{j\mu} + D_i' t_j f_j + A_{ij}'^\mu z_{j\mu}, \quad (\text{A3})$$

$$D_i = -g_\sigma \frac{M_i^*}{p_i^{*0}} \frac{\partial \sigma_i}{\partial \rho_{Si}}, \quad (\text{A4})$$

$$A_{ij}^\mu = \frac{g_\omega^2}{m_\omega^2} B_i B_j z_i^{*\mu}, \quad (\text{A5})$$

$$D_i' = -g_\delta t_i \frac{M_i^*}{p_i^{*0}} \frac{\partial \delta_i}{\partial \rho_{S3,i}}, \quad (\text{A6})$$

$$A_{ij}^\mu = \frac{g_\rho^2}{m_\rho^2} t_i t_j B_i B_j z_i^{*\mu}, \quad (\text{A7})$$

where $z_i^\mu = p_i^\mu / p_i^0$ and $z_i^{*\mu} = p_i^{*\mu} / p_i^{*0}$. Based on Eq. (20), $\frac{\partial \sigma_i}{\partial \rho_{Si}}$ and $\frac{\partial \delta_i}{\partial \rho_{S3,i}}$ are obtained as follows:

$$\frac{\partial \sigma_i}{\partial \rho_{Si}} = \frac{g_\sigma}{m_\sigma^2 + 2g_2 \sigma_i + 3g_3 \sigma_i^2}, \quad \frac{\partial \delta_i}{\partial \rho_{S3,i}} = \frac{g_\delta}{m_\delta^2} \quad (\text{A8})$$

In the two-body center-of-mass frame, ρ_{ij} equals ρ_{ji} . The squared distance $q_{T,ij}^2$ is reduced to $q_{T,ij}^2 \equiv -\vec{r}_{ij}^2 - \frac{(\vec{r}_{ij} \cdot \vec{p}_{ij})^2}{p_{ij}^2}$.

In the actual calculation, we replace p_i^0 with $\sqrt{\vec{p}_i^2 + M_i^2}$ to save calculation time [79]. Thus, the partial derivative of density versus momentum and space can be written as

$$\begin{aligned} \frac{\partial \rho_{ij}}{\partial \vec{p}_i} = -\frac{\rho_{ij}}{2L} \frac{(\vec{r}_{ij} \cdot \vec{p}_{ij}) \cdot \vec{r}_{ij}}{p_{ij}^2} + \rho_{ij} \frac{\gamma_{ij}^2 \vec{\beta}_{ij}}{p_i^0 + p_j^0} [1 - \vec{\beta}_{ij} \frac{\vec{p}_i}{p_i^0}] \\ - \frac{\rho_{ij}}{2L} \frac{(\vec{r}_{ij} \cdot \vec{p}_{ij})^2}{p_{ij}^4} \{ \vec{p}_{ij} - \frac{\vec{p}_i}{p_i^0} p_{ij}^0 \}, \end{aligned} \quad (\text{A9})$$

$$\frac{\partial \rho_{ij}}{\partial \vec{r}_i} = -\frac{\rho_{ij}}{2L} [\vec{r}_{ij} + \frac{(\vec{r}_{ij} \cdot \vec{p}_{ij}) \cdot \vec{p}_{ij}}{p_{ij}^2}], \quad (\text{A10})$$

where $\vec{\beta}_{ij}$ is defined as $(\vec{p}_i + \vec{p}_j) / (p_i^0 + p_j^0)$. In addition, $\frac{\partial f_i}{\partial \vec{p}_i}$ can be written as $-\frac{M_i \vec{p}_i}{p_i^3}$. The partial derivative of the energy component of $\frac{\partial z_{i\mu}}{\partial \vec{p}_i}$ is zero and that of the momentum component of $\frac{\partial z_{i\mu}}{\partial \vec{p}_i}$ is written as $\frac{-p_i^2}{p_i^3}$. Using the above equations, the momentum and space of neutrons and protons are known.

-
- [1] P. Danielewicz, R. Lacey, and W. G. Lynch, Determination of the Equation of State of Dense Matter. *Science*, **298**, 1592(2002). DOI: 10.1126/science.1078070
- [2] B. P. Abbott, R. Abbott, T. D. Abbott et al., Measurements of Neutron Star Radii and Equation of State. *Phys. Rev. Lett.* **121**, 161101 (2018). DOI: <https://doi.org/10.1103/PhysRevLett.121.161101>
- [3] S. Huth, P. T. H. Pang, I. Tews et al., Constraining neutron-star matter with microscopic and macroscopic collisions. *Nature* **606**, 276-280 (2022). DOI: 10.1038/s41586-022-04750-w
- [4] L. W. Chen, Nucl. Symmetry Energy in Nucleon and Quark Matter. *Phys. Rev.*, **34**, 20-28(2017). DOI: 10.11804/NuclPhysRev.34.01.020
- [5] B.A. Li, P.G. Krastev, D.H. Wen et al., Towards understanding astrophysical effects of nuclear symmetry energy. *Eur. Phys. J. A*, **55**, 117(2019). DOI 10.1140/epja/i2019-12780-8
- [6] B.T. Reed, F. J. Fattoyev, C. J. Horowitz, and J. Piekarewicz, Implications of PREX-2 on the Equation of State of Neutron-Rich Matter. *Phys. Rev. Lett.* **126**, 172503(2021). DOI: <https://doi.org/10.1103/PhysRevLett.126.172503>
- [7] J. M. Lattimer, and M. Prakash, Neutron star observations: Prognosis for equation of state Constraints. *Science*, **442**, 109-165 (2007). DOI: [10.1126/science.1151539](https://doi.org/10.1126/science.1151539)
- [8] A. Drago, A. Lavagno, G. Pagliara, and D. Pigato, Early appearance of Δ isobars in neutron stars. *Phys. Rev. C* **90**, 065809 (2014). DOI: <https://doi.org/10.1103/PhysRevC.90.065809>
- [9] J.M. Lattimer and M. Prakash, The equation of state of hot, dense matter and neutron stars, *Phys. Rep.* **621**, 127 (2016). DOI: 10.1016/j.physrep.2015.12.005
- [10] M. Tsang, W. Lynch, P. Danielewicz, and C. Tsang, Symmetry energy constraints from GW170817 and laboratory experiments. *Phys. Lett. B* **795**, 533 (2019). DOI: 10.1016/j.physletb.2019.06.059
- [11] B. Fore and S. Reddy, Pions in hot dense matter and their astrophysical implications. *Phys. Rev. C* **101**, 035809 (2020). DOI: <https://doi.org/10.1103/PhysRevC.101.035809>
- [12] W. B. He, Y. G. Ma, L. G. Pang, H. C. Song, and K. Zhou, High-energy nuclear physics meets machine learning. *Nucl. Sci. Tech.* **34**, 88 (2023). DOI: <https://doi.org/10.1007/s41365-023-01233-z>
- [13] W. Scheid, H. Müller, and W. Greiner, Nuclear Shock Waves in Heavy-Ion Collisions. *Phys. Rev. Lett.* **32**, 741 (1974). DOI: <https://doi.org/10.1103/PhysRevLett.32.741>
- [14] J. Kapusta and D. Strottman, Global analysis of relativistic heavy-ion collisions. *Phys. Lett. B* **106**, 33 (1981). DOI: 10.1016/0370-2693(81)91074-1
- [15] H. Stocker, L. P. Csernai, G. Graebner, G. Buchwald, H. Kruse, R. Y. Cusson, J. A. Maruhn, and W. Greiner, Jets of nuclear

- matter from high energy heavy ion collisions. *Phys. Rev. C* **25**, 1873 (1982). DOI: <https://doi.org/10.1103/PhysRevC.25.1873>
- [16] H. A. Gustafsson, H. H. Gutbrod, B. Kolb et al., Collective Flow Observed in Relativistic Nuclear Collisions. *Phys. Rev. Lett.* **52**, 1590 (1984). DOI: <https://doi.org/10.1103/PhysRevLett.52.1590>
- [17] D. H. Rischke, Y. Pursun, J. A. Maruhn et al., The phase transition to the quark-gluon plasma and its effect on hydrodynamic flow. *Acta Phys. Hung. A* **1**, 309 (1995). DOI: <https://doi.org/10.1007/BF03053749>
- [18] J. Brachmann, S. Soff, A. Dumitru et al., Anti-flow of nucleons at the softest point of the equation of state. *Phys. Rev. C* **61**, 024909 (2000). DOI: <https://doi.org/10.1103/PhysRevC.61.024909>
- [19] L. P. Csernai and D. Rohrlich, Third flow component as QGP signal. *Phys. Lett. B* **458**, 454 (1999). DOI: [10.1016/S0370-2693\(99\)00615-2](https://doi.org/10.1016/S0370-2693(99)00615-2)
- [20] B. A. Li and C. M. Ko, Probing the softest region of the nuclear equation of state. *Phys. Rev. C* **58**, R1382 (1998). DOI: <https://doi.org/10.1103/PhysRevC.58.R1382>
- [21] Y. G. Ma, The Collective Flow from the Degree of Freedom of Nucleons to Quarks. *Journal of Fudan University (Natural Science)* **62**, 273-292 (2023). DOI: [0427-7104\(2023\)03-0273-20](https://doi.org/10.4277/1004(2023)03-0273-20)
- [22] L. Scalone, M. Colonna, and M. Di Toro, Transverse flows in charge asymmetric collisions. *Phys. Lett. B* **461**, 9 (1999). DOI: [10.1016/S0370-2693\(99\)00835-7](https://doi.org/10.1016/S0370-2693(99)00835-7)
- [23] B. A. Li, A. T. Sustich, and B. Zhang, Proton differential elliptic flow and the isospin dependence of the nuclear equation of state. *Phys. Rev. C* **64**, 054604(2001). DOI: <https://doi.org/10.1103/PhysRevC.64.054604>
- [24] Q.F. Li, C.W. Shen, C.C. Guo et al., Nonequilibrium dynamics in heavy-ion collisions at low energies available at the GSI Schwerionen Synchrotron. *Phys. Rev. C* **83**, 044617 (2011). DOI: <https://doi.org/10.1103/PhysRevC.83.044617>
- [25] M. D. Cozma, Neutron-proton elliptic flow difference as a probe for the high density dependence of the symmetry energy. *Phys. Lett. B* **700**, 139 (2011). DOI: [10.1016/j.physletb.2011.05.002](https://doi.org/10.1016/j.physletb.2011.05.002)
- [26] G. Ferini, T. Gaitanos, M. Colonna et al., Isospin Effects on Subthreshold Kaon Production at Intermediate Energies. *Phys. Rev. Lett.* **97**, 202301 (2006). DOI: <https://doi.org/10.1103/PhysRevLett.97.202301>
- [27] B. A. Li, Probing the High Density Behavior of the Nuclear Symmetry Energy with High Energy Heavy-Ion Collisions. *Phys. Rev. Lett.* **88**, 192701 (2002). DOI: <https://doi.org/10.1103/PhysRevLett.88.192701>
- [28] T. Gaitanos, M. Di Toro, S. Typel et al., On the Lorentz structure of the symmetry energy. *Nucl. Phys. A* **732**, 24 (2004). DOI: [10.1016/j.nuclphysa.2003.12.001](https://doi.org/10.1016/j.nuclphysa.2003.12.001)
- [29] C. Sturm, I. Bottcher, M. Debowski, A. Forster, E. Grosse, P. Koczon, and B. Kollmeier, *et al.*, (KaoS Collaboration), Evidence for a Soft Nuclear Equation-of-State from Kaon Production in Heavy-Ion Collisions. *Phys. Rev. Lett.* **86**, 39 (2001). DOI: <https://doi.org/10.1103/PhysRevLett.86.39>
- [30] G. Q. Li and C. M. Ko, Subthreshold kaon production and the nuclear equation of state. *Phys. Lett. B* **349**, 405 (1995). DOI: [10.1016/0370-2693\(95\)00301-Z](https://doi.org/10.1016/0370-2693(95)00301-Z)
- [31] C. Fuchs, A. Faessler, E. Zabrodin et al., Probing the Nuclear Equation of State by K^+ Production in Heavy-Ion Collisions. *Phys. Rev. Lett.* **86**, 1974 (2001). DOI: <https://doi.org/10.1103/PhysRevLett.86.1974>
- [32] C. Hartnack, H. Oeschler, and J. Aichelin, Hadronic Matter Is Soft. *Phys. Rev. Lett.* **96**, 012302 (2006). DOI: <https://doi.org/10.1103/PhysRevLett.96.012302>
- [33] Z. Q. Feng, Constraining the high-density behavior of the nuclear equation of state from strangeness production in heavy-ion collisions. *Phys. Rev. C* **83**, 067604 (2011). DOI: <https://doi.org/10.1103/PhysRevC.83.067604>
- [34] Z. Q. Feng and G. M. Jin, Probing high-density behavior of symmetry energy from pion emission in heavy-ion collisions. *Phys. Lett. B* **683**, 140 (2010). DOI: [10.1016/j.physletb.2009.12.006](https://doi.org/10.1016/j.physletb.2009.12.006)
- [35] P. Russotto, P. Z. Wu, M. Zoric *et al.*, Symmetry energy from elliptic flow in 197Au+ 197Au. *Phys. Lett. B* **697**, 471 (2011). DOI: [10.1016/j.physletb.2011.02.033](https://doi.org/10.1016/j.physletb.2011.02.033)
- [36] Z. G. Xiao, B. A. Li, L. W. Chen, G. C. Yong, and M. Zhang, Circumstantial Evidence for a Soft Nuclear Symmetry Energy at Suprasaturation Densities. *Phys. Rev. Lett.* **102**, 062502 (2009). DOI: <https://doi.org/10.1103/PhysRevLett.102.062502>
- [37] W. J. Xie, J. Su, L. Zhu, and F. S. Zhang, Symmetry energy and pion production in the Boltzmann-Langevin approach. *Phys. Lett. B* **718**, 1510 (2013). DOI: [10.1016/j.physletb.2012.12.021](https://doi.org/10.1016/j.physletb.2012.12.021)
- [38] W. Reisdorf, M. Stockmeier, A. Andronic, M. L. Benabderahmane, O. N. Hartmann, and N. Herrmann, *et al.*, Systematics of pion emission in heavy ion collisions in the 1 A GeV regime. *Nucl. Phys. A* **781**, 459 (2007). DOI: [10.1016/j.nuclphysa.2006.10.085](https://doi.org/10.1016/j.nuclphysa.2006.10.085)
- [39] G. Jhang, J. Estee, J. Barney, G. Cerizza, and M. Kaneko, *et al.*, Symmetry energy investigation with pion production from Sn+ Sn systems. *Phys. Lett. B* **813**, 136016 (2021). DOI: [10.1016/j.physletb.2020.136016](https://doi.org/10.1016/j.physletb.2020.136016)
- [40] J. Estee, W.G. Lynch, C.Y. Tsang, J. Barney, G. Jhang, M.B. Tsang, and R. Wang, *et al.*, Probing the Symmetry Energy with the Spectral Pion Ratio. *Phys. Rev. Lett.* **126**, 162701 (2021). DOI: <https://doi.org/10.1103/PhysRevLett.126.162701>
- [41] G. F. Wei, X. Huang, Q. J. Zhi, A. J. Dong, C. G. Peng, and Z. W. Long, Effects of the momentum dependence of nuclear symmetry potential on pion observables in Sn plus Sn collisions at 270 MeV/nucleon. *Nucl. Sci. Tech.* **33**, 163 (2022). DOI: [10.1007/s41365-022-01146-3](https://doi.org/10.1007/s41365-022-01146-3)
- [42] H. Sorge, H. Stöcker, and W. Greiner, Poincare invariant Hamiltonian dynamics: modelling multi-hadronic interactions in a phase space approach. *Ann. Phys.* **192**, 266 (1989). DOI: [10.1016/0003-4916\(89\)90136-X](https://doi.org/10.1016/0003-4916(89)90136-X)
- [43] T. Maruyama, S. W. Huang, N. Ohtsuka, G. Li, and A. Faessler, Lorentz-covariant description of intermediate energy heavy-ion reactions in relativistic quantum molecular dynamics. *Nucl. Phys. A* **534**, 720 (1991). DOI: [10.1016/0375-9474\(91\)90468-L](https://doi.org/10.1016/0375-9474(91)90468-L)
- [44] Y. Nara and H. Stoecker, Sensitivity of the excitation functions of collective flow to relativistic scalar and vector meson interactions in the relativistic quantum molecular dynamics model RQMD.RMF. *Phys. Rev. C* **100**, 054902 (2019). DOI: <https://doi.org/10.1103/PhysRevC.100.054902>
- [45] Y. Nara, T. Maruyama, and H. Stoecker, Momentum-dependent potential and collective flows within the relativistic quantum molecular dynamics approach based on relativistic mean-field theory. *Phys. Rev. C* **102**, 024913 (2020). DOI: <https://doi.org/10.1103/PhysRevC.102.024913>
- [46] Y. Nara, A. Jinno, K. Murase, and A. Ohnishi, Directed flow of Λ in high-energy heavy-ion collisions and Λ potential in dense nuclear matter. *Phys. Rev. C* **106**, 044902 (2022).
- [47] Z. Q. Feng and G. M. Jin, Pion production in heavy-ion collisions in the 1 A GeV region. *Chin. Phys. Lett.* **26**, 062501(2009). DOI: [10.1088/0256-307X/26/6/062501](https://doi.org/10.1088/0256-307X/26/6/062501)

- [48] Z. Q. Feng, W. J. Xie, P. H. Chen, J. Chen, and G. M. Jin, In-medium and isospin effects on particle production near threshold energies in heavy-ion collisions. *Phys. Rev. C* **92**, 044604 (2015). DOI: <https://doi.org/10.1103/PhysRevC.92.044604>
- [49] Z. Q. Feng, Nuclear dynamics and particle production near threshold energies in heavy-ion collisions. *Nucl. Sci. Tech.* **29**, 40 (2018). DOI: [10.1007/s41365-018-0379-z](https://doi.org/10.1007/s41365-018-0379-z)
- [50] Z. Q. Feng, H. J. Liu, H. G. Cheng, and S. N. Wei, Progress in strange particle production and hypernuclear physics in intermediate and high-energy heavy-ion collisions. *Nucl. Tech.* **46**, 103-113(2023). DOI: [10.11889/j.0253-3219.2023.hjs.46.080010](https://doi.org/10.11889/j.0253-3219.2023.hjs.46.080010)
- [51] M. H. Zhang, Y. H. Zhang, J. J. Li, N. Tang, S. Sun, and F. S. Zhang, Progress in transport models of heavy-ion collisions for the synthesis of superheavy nuclei. *Nucl. Tech.* **46**, 137-145(2023). DOI: [10.11889/j.0253-3219.2023.hjs.46.080014](https://doi.org/10.11889/j.0253-3219.2023.hjs.46.080014)
- [52] Y. G. Ma, Effects of α -clustering structure on nuclear reaction and relativistic heavy-ion collisions. *Nucl. Tech.* **46**, 8-29 (2023). DOI: [10.11889/j.0253-3219.2023.hjs.46.080001](https://doi.org/10.11889/j.0253-3219.2023.hjs.46.080001)
- [53] P. C. Li, Y. J. Wang, Q. F. Li, and H. F. Zhang, Transport model analysis of the pion interferometry in Au+Au collisions at $E_{beam}=1.23$ GeV/nucleon. *Sci. China-Phys. Mech. Astron.* **66**, 222011(2023). DOI: <https://doi.org/10.1007/s11433-022-2026-5>
- [54] P. C. Li, J. Steinheimer, T. Reichert, A. Kittiratpattana, M. Bleicher, and Q. F. Li, Effects of a phase transition on two-pion interferometry in heavy ion collisions at $\sqrt{s_{NN}}=2.4-7.7$ GeV. *Sci. China-Phys. Mech. Astron.* **66**, 232011(2023). DOI: <https://doi.org/10.1007/s11433-022-2041-8>
- [55] K. Xiao, P. C. Li, Y. J. Wang, F. H. Liu, and Q. F. Li, Effects of sequential decay on collective flows and nuclear stopping power in heavy-ion collisions at intermediate energies. *Nucl. Sci. Tech.* **34**, 62(2023). DOI: <https://doi.org/10.1007/s41365-023-01205-3>
- [56] J. D. Walecka, A theory of highly condensed matter. *Ann. Phys.* **83**, 491(1974). DOI: [10.1016/0003-4916\(74\)90208-5](https://doi.org/10.1016/0003-4916(74)90208-5)
- [57] J. Boguta, and A. R. Bodmer, Relativistic calculation of nuclear matter and the nuclear surface. *Nucl. Phys. A* **292**, 413(1977). DOI: [10.1016/0375-9474\(77\)90626-1](https://doi.org/10.1016/0375-9474(77)90626-1)
- [58] B. D. Serot, A relativistic nuclear field theory with pi and rho mesons. *Phys. Lett. B* **86B**, 146 (1979). DOI: [10.1016/0370-2693\(79\)90804-9](https://doi.org/10.1016/0370-2693(79)90804-9)
- [59] S. Kubis, and M. Kutschera, Nuclear matter in relativistic mean field theory with isovector scalar meson. *Phys. Lett. B* **399**, 191 (1997). DOI: [10.1016/S0370-2693\(97\)00306-7](https://doi.org/10.1016/S0370-2693(97)00306-7)
- [60] B. Liu, V. Greco, V. Baran, M. Colonna, and M. Di Toro, Asymmetric nuclear matter: The role of the isovector scalar channel. *Phys. Rev. C* **65**, 045201 (2002). DOI: <https://doi.org/10.1103/PhysRevC.65.045201>
- [61] C. Xu, B. A. Li, and L. W. Chen, Symmetry energy, its density slope, and neutron-proton effective mass splitting at normal density extracted from global nucleon optical potentials. *Phys. Rev. C* **82**, 054607 (2010). DOI: <https://doi.org/10.1103/PhysRevC.82.054607>
- [62] X. H. Li, W. J. Guo, B. A. Li, L. W. Chen, F. J. Fattoyev, and W. G. Newton, Neutron-proton effective mass splitting in neutron-rich matter at normal density from analyzing nucleon-nucleus scattering data within an isospin dependent optical model. *Phys. Lett. B* **743**, 408 (2015). DOI: [10.1016/j.physletb.2015.03.005](https://doi.org/10.1016/j.physletb.2015.03.005)
- [63] W. Zuo, I. Bombaci, and U. Lombardo, Asymmetric nuclear matter from an extended Brueckner-Hartree-Fock approach. *Phys. Rev. C* **60**, 024605 (1999). DOI: <https://doi.org/10.1103/PhysRevC.60.024605>
- [64] Z. Y. Ma, J. Rong, B. Q. Chen, Z. Y. Zhu, and H. Q. Song, Isospin dependence of nucleon effective mass in Dirac Brueckner-Hartree-Fock approach. *Phys. Lett. B* **604**, 170 (2004). DOI: [10.1016/j.physletb.2004.11.004](https://doi.org/10.1016/j.physletb.2004.11.004)
- [65] E. N. E. van Dalen, C. Fuchs, and A. Faessler, Effective Nucleon Masses in Symmetric and Asymmetric Nuclear Matter. *Phys. Rev. Lett.* **95**, 022302 (2005). DOI: <https://doi.org/10.1103/PhysRevLett.95.022302>
- [66] W. H. Long, N. Van Giai, and J. Meng, Density-dependent relativistic Hartree-Fock approach. *Phys. Lett. B* **640**, 150 (2006). DOI: [10.1016/j.physletb.2006.07.064](https://doi.org/10.1016/j.physletb.2006.07.064)
- [67] D. D. S. Coupland, M. Youngs, Z. Chajecski, *et al.*, Probing effective nucleon masses with heavy-ion collisions. *Phys. Rev. C* **94**, 011601 (2016). DOI: <https://doi.org/10.1103/PhysRevC.94.011601>
- [68] P. Morfouace, C. Y. Tsang, Y. Zhang, *et al.*, Constraining the symmetry energy with heavy-ion collisions and Bayesian analyses. *Phys. Lett. B* **799**, 135045 (2019). DOI: [10.1016/j.physletb.2019.135045](https://doi.org/10.1016/j.physletb.2019.135045)
- [69] L. W. Chen, C. M. Ko, and B. A. Li, Isospin-dependent properties of asymmetric nuclear matter in relativistic mean field models. *Phys. Rev. C* **76**, 054316 (2007). DOI: <https://doi.org/10.1103/PhysRevC.76.054316>
- [70] V. Baran, M. Colonna, V. Greco, and M. Di Toro, Reaction dynamics with exotic nuclei. *Phys. Rep.* **410**, 335 (2005). DOI: [10.1016/j.physrep.2004.12.004](https://doi.org/10.1016/j.physrep.2004.12.004)
- [71] M. Dutra, O. Lourenco, J. S. S. Martins, A. Delfino, J. R. Stone, and P. D. Stevenson, Skyrme interaction and nuclear matter constraints. *Phys. Rev. C* **85**, 035201 (2012). DOI: <https://doi.org/10.1103/PhysRevC.85.035201>
- [72] R. Sellaheewa and A. Rios, Isovector properties of the Gogny interaction. *Phys. Rev. C* **90**, 054327 (2014). DOI: <https://doi.org/10.1103/PhysRevC.90.054327>
- [73] L. Ou, Z. X. Li, Y. X. Zhang, and M. Liu, Effect of the splitting of the neutron and proton effective masses on the nuclear symmetry energy at finite temperatures. *Phys. Lett. B* **697**, 246 (2011). DOI: [10.1016/j.physletb.2011.01.062](https://doi.org/10.1016/j.physletb.2011.01.062)
- [74] S. Goriely, S. Hilaire, M. Girod, and S. Pru, First Gogny-Hartree-Fock-Bogoliubov Nuclear Mass Model. *Phys. Rev. Lett.* **102**, 242501 (2009). DOI: <https://doi.org/10.1103/PhysRevLett.102.242501>
- [75] Z. Zhang, and L. W. Chen, Isospin splitting of the nucleon effective mass from giant resonances in 208Pb. *Phys. Rev. C* **93**, 034335 (2016). DOI: <https://doi.org/10.1103/PhysRevC.93.034335>
- [76] Z. Zhang, X. B. Feng, and L. W. Chen, Bayesian inference on isospin splitting of nucleon effective mass from giant resonances in 208Pb. *Chin. Phys. C* **45**, 064104 (2021). DOI: [10.1088/1674-1137/abf428](https://doi.org/10.1088/1674-1137/abf428)
- [77] R. Marty, and J. Aichelin, Molecular dynamics description of an expanding q/\bar{q} plasma with the Nambu-Jona-Lasinio model and applications to heavy ion collisions at energies available at the BNL Relativistic Heavy Ion Collider and the CERN Large Hadron Collider. *Phys. Rev. C* **87**, 034912 (2013). DOI: <https://doi.org/10.1103/PhysRevC.87.034912>
- [78] A. Komar, Constraint formalism of classical mechanics. *Phys. Rev. D* **18**, 1881 (1978). DOI: <https://doi.org/10.1103/PhysRevD.18.1881>
- [79] M. Isse, A. Ohnishi, N. Otuka, P. K. Sahu, and Y. Nara, Mean-field effects on collective flow in high-energy heavy-ion collisions at 2-158A GeV energies. *Phys. Rev. C* **72**, 064908 (2005). DOI: <https://doi.org/10.1103/PhysRevC.72.064908>
- [80] E. C. G. Sudarshan, N. Mukunda, and J. N. Goldberg, Con-

- straint dynamics of particle world lines. Phys. Rev. D **23**, 2218 (1981). DOI: <https://doi.org/10.1103/PhysRevD.23.2218>
- [81] D. Oliinychenko, and H. Petersen, Deviations of the energy-momentum tensor from equilibrium in the initial state for hydrodynamics from transport approaches. Phys. Rev. C **93**, 034905 (2016). DOI: <https://doi.org/10.1103/PhysRevC.93.034905>
- [82] G. E. Brown and W. Weise, Pion scattering and isobars in nuclei. Phys. Rep. **22**, 279 (1975). DOI: [10.1016/0370-1573\(75\)90026-5](https://doi.org/10.1016/0370-1573(75)90026-5)
- [83] B. Friemann, V. P. Pandharipande, and Q. N. Usmani, Very hot nuclear matter and pion production in relativistic heavy-ion collisions. Nucl. Phys. A **372**, 483 (1981). DOI: [10.1016/0375-9474\(81\)90048-8](https://doi.org/10.1016/0375-9474(81)90048-8)
- [84] L. Xiong, C. M. Ko, and V. Koch, Transport model with quasipions. Phys. Rev. C **47**, 788 (1993). DOI: <https://doi.org/10.1103/PhysRevC.47.788>
- [85] G. Ferini, M. Colonna, T. Gaitanos, and M. Di Toro, Aspects of particle production in isospin-asymmetric matter. Nucl. Phys. A **762**, 147 (2005). DOI: [10.1016/j.nuclphysa.2005.08.007](https://doi.org/10.1016/j.nuclphysa.2005.08.007)
- [86] T. Song, and C. M. Ko, Modifications of the pion-production threshold in the nuclear medium in heavy ion collisions and the nuclear symmetry energy. Phys. Rev. C **91**, 014901 (2015). DOI: <https://doi.org/10.1103/PhysRevC.91.014901>
- [87] M.D. Cozma, The impact of energy conservation in transport models on the π^-/π^+ multiplicity ratio in heavy-ion collisions and the symmetry energy. Phys. Lett. B **753**, 166-172 (2016). DOI: [10.1016/j.physletb.2015.12.015](https://doi.org/10.1016/j.physletb.2015.12.015)
- [88] Z. Q. Feng, Nuclear in-medium effects and collective flows in heavy-ion collisions at intermediate energies. Phys. Rev. C **85**, 014604 (2012). DOI: <https://doi.org/10.1103/PhysRevC.85.014604>
- [89] Z. Q. Feng, Nuclear fragmentation and charge-exchange reactions induced by pions in the Δ -resonance region. Phys. Rev. C **94**, 054617 (2016). DOI: <https://doi.org/10.1103/PhysRevC.94.054617>
- [90] M. S. Abdallah, *et al.* (STAR Collaboration), Disappearance of partonic collectivity in $\sqrt{s_{NN}}=3$ GeV Au+Au collisions at RHIC. Phys. Lett. B **827**, 137003 (2022). DOI: [10.1016/j.physletb.2022.137003](https://doi.org/10.1016/j.physletb.2022.137003)
- [91] S. Huber, and J. Aichelin, Production of Δ - and N^* -resonances in the one-boson exchange model. Nucl. Phys. A **573**, 587 (1994). DOI: [10.1016/0375-9474\(94\)90232-1](https://doi.org/10.1016/0375-9474(94)90232-1)
- [92] B. A. Li, A. T. Sustich, B. Zhang, and C. M. Ko, STUDIES OF SUPERDENSE HADRONIC MATTER IN A RELATIVISTIC TRANSPORT MODEL. Int. J. Mod. Phys. E **10**, 267 (2001). DOI: <https://doi.org/10.1142/S0218301301000575>
- [93] E. Chabanat, R. Bonche, R. Haensel, J. Meyer, and R. Schaeffer, A Skyrme parametrization from subnuclear to neutron star densities Part II. Nuclei far from stabilities. Nucl. Phys. A **635**, 231-256 (1998). DOI: [10.1016/S0375-9474\(98\)00180-8](https://doi.org/10.1016/S0375-9474(98)00180-8)
- [94] Z. Q. Feng, G. M. Jin, and F. S. Zhang, Dynamical analysis on heavy-ion fusion reactions near Coulomb barrier. Nucl. Phys. A **802**, 91-106 (2008). DOI: [10.1016/j.nuclphysa.2008.01.022](https://doi.org/10.1016/j.nuclphysa.2008.01.022)
- [95] V. Giordano, M. Colonna, M. Di Toro, V. Greco, and J. Rizzo, Isospin emission and flow at high baryon density: A test of the symmetry potential. Phys. Rev. C **81**, 044611 (2010). DOI: <https://doi.org/10.1103/PhysRevC.81.044611>